metals

MDPI

Article

Heat Treatment Effect on Microstructure Evolution in a 7% Cr Steel for Forging

Andrea Di Schino [1,*], Matteo Gaggiotti [1] and Claudio Testani [2]

[1] Engineering Department, University of Perugia, Via G. Duranti 93, 06125 Perugia, Italy; matteo.gaggiotti@studenti.unipg.it

[2] CALEF-ENEA CR Casaccia, Via Anguillarese 301, Santa Maria di Galeria, 00123 Rome, Italy; claudio.testani@consorziocalef.it

* Correspondence: andrea.dischino@unipg.it

Received: 25 May 2020; Accepted: 16 June 2020; Published: 17 June 2020

Abstract: Well-defined heat-treatment guidelines are required to achieve the target mechanical properties in high-chromium steels for forgings. Moreover, for this class of materials, the microstructure evolution during heat treatment is not clearly understood. Thus, it is particularly important to assess the steel microstructure evolution during heat treatment, in order to promote the best microstructure. This will ascertain the safe use for long-term service. In this paper, different heat treatments are considered, and their effect on a 7% Cr steel for forging is reported. Results show that, following the high intrinsic steel hardenability, significative differences were not found versus the cooling-step treatment, although prior austenite grain size was significantly different. Moreover, retained austenite (RA) content is lower in double-tempered specimens after heat treatments at higher temperatures.

Keywords: forged steels; microstructure; high-Cr steel

1. Introduction

In the energy industry, every steel component is asked to have a long service duration (often longer than 30 years). The possibility to produce forged steel components characterized by high mechanical properties and competitive costs has gained more and more importance in the last years.

Medium-carbon steels have been widely used for primary energy-plant-production applications due to their excellent performances. This often needs to face with strong requirements in terms of severe service conditions (high temperature, high pressures, corrosion issues, nuclear irradiation, etc.) [1–4].

In the case of energy-sector applications (especially in oil and gas), corrosion resistance issues are often coupled with demanding mechanical requirements: in such cases, carbon steel is often cladded with stainless steels or even nickel superalloys [5–7].

Concerning mechanical properties, it is well-known that they strongly depend on grain size and steel alloying (through solution and precipitation hardening mechanisms), as discussed in the literature. Morito et al., reported the effect of microstructure refining [8]; Fan et al., discussed microstructural and precipitation effect on high-chromium steels microstructure [9]; Akbarzadeh et al., studied the hot workability of high-carbon and high-chromium steel [10]. The microstructure evolution in medium-carbon steel is well described in Reference [11], and the phase transformation evolution in high-strength low-alloyed steels is reported in Reference [12]. Some authors reported that limited amounts of retained austenite have a beneficial effect on mechanical properties [13]. It is reported that grain-size refinement should increase the yield strength up to three times [14–16]. Moreover, such a strengthening mechanism can allow the best balance of strength/toughness combination [17–19].

Solution-hardening mechanisms, if properly activated by the addition of elements, allows us to increase the wear, fatigue and high-temperature behavior [20–23].

As far as microstructure refinement is concerned, in recent years, there has been an intense focus on plastic-deformation processes, such us forging technologies [24–27]. In fact, it is reported that forging is a method for grain-size refinement via plastic-deformation accumulation. This enhances the material strength and toughness. The raw materials' internal cracks and defects can be reduced during forging, as well as mean grain size, thus allowing for a more uniform grain-size distribution [28,29]. Chaudhari et al. [30–33] reported that the grain size is clearly refined after steel multidirectional forging. This leads to the formation of fine austenite grains following the activation of continuous dynamic recrystallization and dynamic recovery. They showed that fine grains' formation is beneficial in terms of tensile strength and hardness enhancement. Gosh et al. [34] outlined that the material mechanical properties' best combination is found in the case of pure ferrite microstructure.

In high-Cr-bearing steels micro-alloying strengthening phenomena are reported to be effective to refine grains during thermomechanical processing. Kvackaj et al., analyzed austenite deformation behavior during thermomechanical processing of Nb–Ti micro-alloyed steel. They studied thermomechanical cycles aimed to favor the formation of (i) recrystallized austenite, (ii) un-recrystallized austenite, and (iii) ferrite-pearlite microstructures [35]. De Ardo reported micro-alloyed forged steels, emphasizing the possibility that pearlite-ferrite microstructures (formed during air cooling) can exhibit final strengths and fatigue resistances similar to those of the more expensive heat-treated steel [36]. Opiela reported the effect of thermomechanical processing on the microstructure and mechanical properties of Nb-Ti-V micro-alloyed steel [37]. Di Schino reported forging simulation and microstructure evolution of large-scale ingot in micro-alloyed tool steel [38]. Zitelli et al., recently discussed vanadium micro-alloyed steels for large-scale forged ingots, with the aim to balance production costs with the industrial demand of forged steels with high tensile properties. They demonstrated, at a laboratory scale, that ASTM A694 F70 forged-steel grade requirements can be fulfilled by a vanadium micro-alloyed steel with an addition of 0.15% V (plus proper heat treatment), consisting of a ferrite-pearlite microstructure [39]. Mancini et al., reported defect reduction and quality optimization by modeling plastic deformation and metallurgical evolution in ferritic stainless steels [40]. Moreover, substitutional strengthening mechanism in 7–12% Cr carbon alloyed steels has been widely studied and proved to have an excellent mechanical properties combination [41–44]. Among them, 7% Cr steels are nowadays proposed by many steelmakers for being quite promising in terms of properties/cost combination instead of the more common 9–12% steels.

Commonly, after casting, the steel ingots are deformed (forging) and heat treated. Such heat treatment, called preheating treatment or after-forging heat treatment, is aimed to develop the target microstructure for the desired mechanical properties. Finally, the heat-treatment sequence for high Cr steels (also called quality heat treatment) includes austenitization, followed by quenching and high-temperature tempering (Q & T). The microstructure of the final products typically consists of tempered martensite, undissolved carbonitrides, and/or re-precipitated carbonitrides [45]. The austenitizing temperature and soaking time determines the partitioning of carbon and alloying elements between the austenite and carbonitrides. In this processing step, a temperature increase leads to an increase of the carbonitrides dissolution degree with a positive effect on the mechanical properties [46–48]. After austenitization, cooling to below the martensite start temperature (M_s) leads to martensite formation. In its as-quenched martensitic condition, the steel is hard and brittle and may contain "pockets" of retained austenite (RA). The quenching step is followed by a high-temperature tempering step (in the range of 500–650 °C), to reduce brittleness and increase ductility and toughness by reducing residual stresses. All the parameters involved in a particular heat-treatment process strongly affect the steel final microstructure, e.g., austenitization temperature, holding time, quench medium, cooling rate, tempering temperature, and holding time. Well-defined heat-treatment guidelines are therefore required to assist the manufacturer in the selection of the correct heat treatment for achieving the target properties.

Ultimately, the microstructure evolution during the heat treatment of high-Cr steels is still not clearly understood. Thus, the understanding of microstructure evolution during heat treatment in wt.% Cr steel became a key factor for a safe long-term-service steel-microstructure design.

In this paper, the heat-treatment effect on a 7% Cr steel for forging is reported. Different heat treatments are considered. The resulting microstructure evolution is analyzed.

2. Materials and Methods

The steel nominal chemical composition is reported in Table 1.

Table 1. Main chemical composition of the considered materials (mass, %).

C	Cr	Mo	Mn	Ni	Si	V	Fe
0.42	7.0	0.70	0.65	<0.20	0.50	0.10	Balance

Specimens were withdrawn, starting from a sample-ingot for Continuous Cooling Temperature (CCT) diagrams determination. CCT diagrams were derived based on the dilatometry experiments carried out on 10 mm in length, 6 mm in diameter specimens, with controlled cooling rate. Microstructure analysis and hardness measurements of heat-treated specimens were performed by means of Light Microscopy (LM), after 4% Nital etching and Brinell indenter (HB). Prior austenite grain size was measured by image analysis software after samples etching in 10 g of CrO_3, 50 g of NaOH, 1.5 g of picric acid, and 100 mL of distilled water solution, at room temperature, for 20 s. After etching, specimens were cleaned and dried.

The following heat treatments' cycles were the performed by means of dilatometer (Table 2 and Figure 1).

Heat treatments were designed with the aim to obtain different microstructures in terms of retained austenite content. Austenite transformation during the different steps of a laboratory manufacturing route that is reproducing an industrially relevant process was considered. In particular, the following four microstructural families were targeted:

(1) Quenching and partitioning (specimen Q & P): Such heat treatment is here investigated based on very promising results reported on its effect on 9% Cr steels [49].
(2) Partially transforming austenite during first quenching at 280 °C (specimens *n*. PT-γ-1 to PT-γ-4).
(3) Partially transforming austenite during secondary cooling at 220 °C (specimens *n*. PT-γ-5 to PT-γ-8).
(4) Quenching (specimens Q, 100% martensite), quenching and tempering (specimens Q & T).
(5) Specimens PT-γ-1 and PT-γ-5 did not undergo any tempering; specimens PT-γ-2 and PT-γ-6 just underwent first tempering treatment at 533 °C; specimens PT-γ-3 and PT-γ-7 were subjected to second tempering at 528 °C; specimens PT-γ-4 and PT-γ-6 were subjected to second tempering at 505 °C.

In order to investigate the possible presence of retained austenite, X-Ray Diffraction (XRD) measurements were performed on heat-treated specimens. XRD analysis was carried out, using a Siemens D500 diffractometer (Siemens, Munich, Germany) equipped with Co-tube radiation and a graphite-monochromator on the detector side, with step size (2θ) of 0.05° and counting time of 5 s/step. The effect of possible texture was eliminated by a rotating fixture on the goniometer. Since low RA contents are expected in this class of steels, facing with XRD technique sensitivity, particular attention has been devoted to spectra postprocessing analysis. In particular, in order to avoid peaks overlapping, and thus to extract information also from "hidden peaks", spectra were processed by a tool specifically developed for peaks deconvolution (Figure 2). Three specimens were analyzed for each heat-treatment condition.

Table 2. Heat treatments' sequence.

Nr	Austenitization		Interrupted Quenching		Heating		Cooling down to
	T **(°C)**	***t*** **(s)**	***T*** **(°C)**	***t*** **(s)**	***T*** **(°C)**	***t*** **(s)**	
Q & P	980	10,800	150	3600	450	3600	12 °C/h up to 220 °C
PT-γ-1			280				12 °C/h up to 220 °C
PT-γ-2							12 °C/h up to 220 °C
PT-γ-3							12 °C/h up to 220 °C
PT-γ-4							12 °C/h up to 220 °C
PT-γ-5			400				12 °C/h up to 220 °C
PT-γ-6							12 °C/h up to 220 °C
PT-γ-7							12 °C/h up to 220 °C
PT-γ-8							12 °C/h up to 220 °C

Nr	First Tempering		Cooling down to		Second Tempering		Cooling down to
	T **(°C)**	***t*** **(s)**	***T*** **(°C)**	***t*** **(s)**	***T*** **(°C)**	***t*** **(s)**	
Q & P	505 °C × 57,600 s		300 °C/3600 s		505 °C × 57,600 s		Room temperature
PT-γ-1	No tempering				No tempering		
PT-γ-2	533 °C × 57,600 s				No tempering		
PT-γ-3	533 °C × 57,600 s				528 °C × 57,600 s		
PT-γ-4	505 °C × 57,600 s				505 °C × 57,600 s		
PT-γ-5	No tempering				No tempering		
PT-γ-6	533 °C × 57,600 s				No tempering		
PT-γ-7	533 °C × 57,600 s				528 °C × 57,600 s		
PT-γ-8	505 °C × 57,600 s				505 °C × 57,600 s		

Nr	Austenitization	Quenched to	First Tempering	Second Tempering
Q	980 °C × 3600 s	RT		
Q & T		RT	533 °C × 57,600 s	528 °C × 57,600 s

Electron Backscattered Diffraction (EBSD) measurements were performed in selected cases, with the aim to detect the presence and position of retained austenite islands, by means of a JEOL field emission gun scanning electron microscope (FEG-SEM) (JEOL Ltd., Tokyo, Japan), using a 0.12 μm scanning step size. Retained austenite was revealed by building up phase maps, taking into account both face-centered cube (fcc) and body-centered cube (bcc) phases: automatic image analysis of such maps allowed us to determine retained austenite volume fraction. The precipitation state was analyzed by transmission electron microscope (TEM) on extraction replica specimens. The observations were performed with a JEOL 200CX transmission electron microscopy (JEOL Ltd., Tokyo, Japan). The hardness dependence upon heat treatments was assessed by means of Brinell hardness measurements.

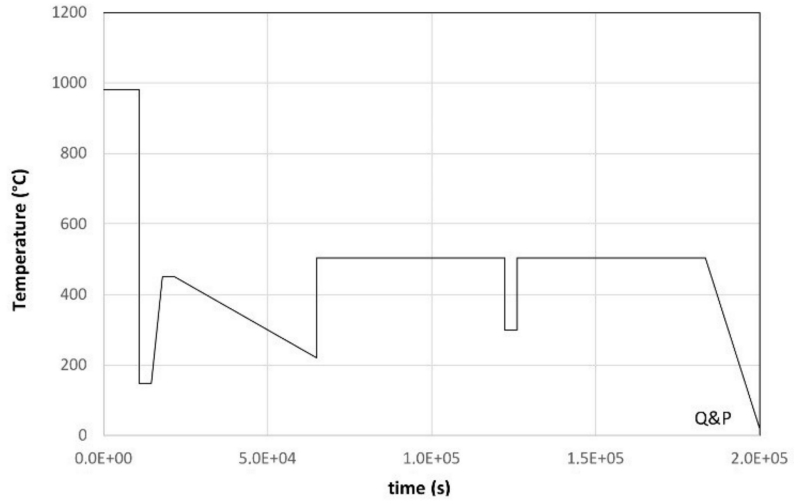

(**a**)

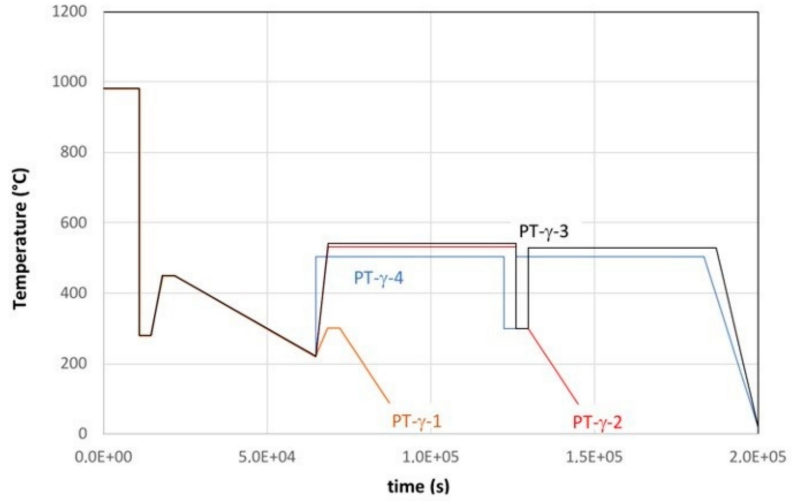

(**b**)

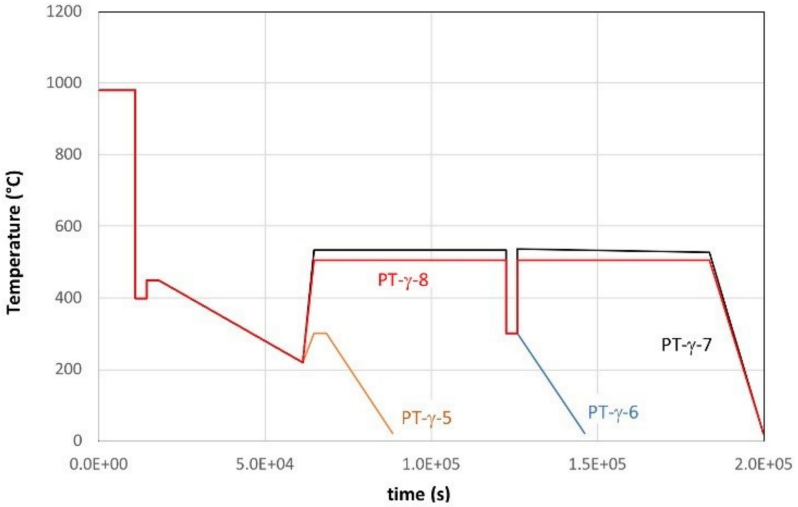

(**c**)

Figure 1. (**a**) Heat-treatment cycle as performed on Q & P specimen; (**b**) heat-treatment cycle as performed on specimens from PT-γ-1 to PT-γ-4; (**c**) heat-treatment cycle as performed on specimens from PT-γ-5 to PT-γ-8.

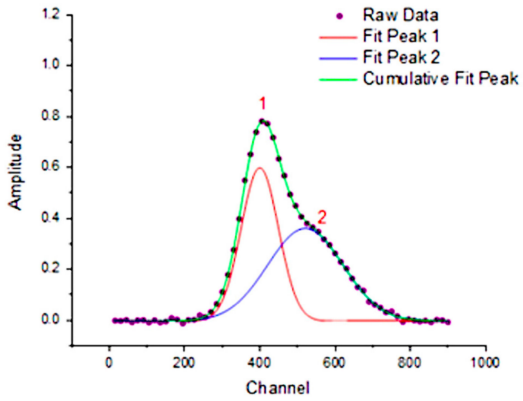

Figure 2. Example of XRD peak deconvolution.

3. Results and Discussion

3.1. Continuous Cooling Transformation

CCT diagrams were determined after austenitization at two different temperatures: 980 and 1200 °C. The first temperature is typical of that commonly adopted during quality heat treatments, and the second one of the final forging-process passes (before cooling). A 30 min soaking time was considered. Dilatometric curves acquired in order to build up the steel CCT are reported in Figures 3 and 4, respectively. The green cooling curve reported in Figure 4 represents the first cooling undergone by all specimens reported in Table 2. This assures that, in the case of complete quenching, a fully martensitic microstructure was achieved (specimens Q and Q & T). On the other hand, this also assures that, in the case of partial quenching, a mixed martensite–austenite microstructure is obtained (specimens Q & P and PT-γ-1 to PT-γ-8).

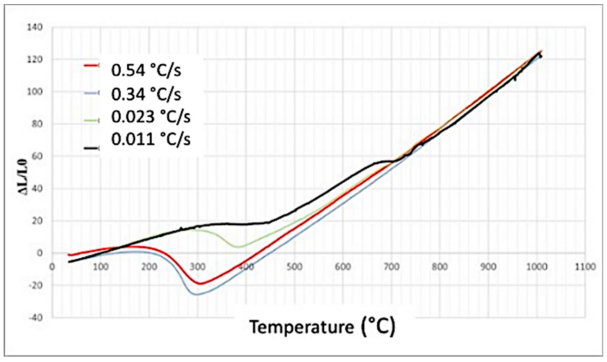

(**a**)

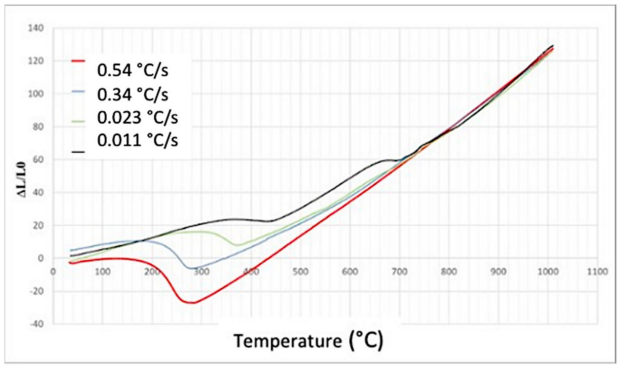

(**b**)

Figure 3. Dilatometric curves of the considered steel: (**a**) austenitization at 980 °C; (**b**) austenitization at 1200 °C.

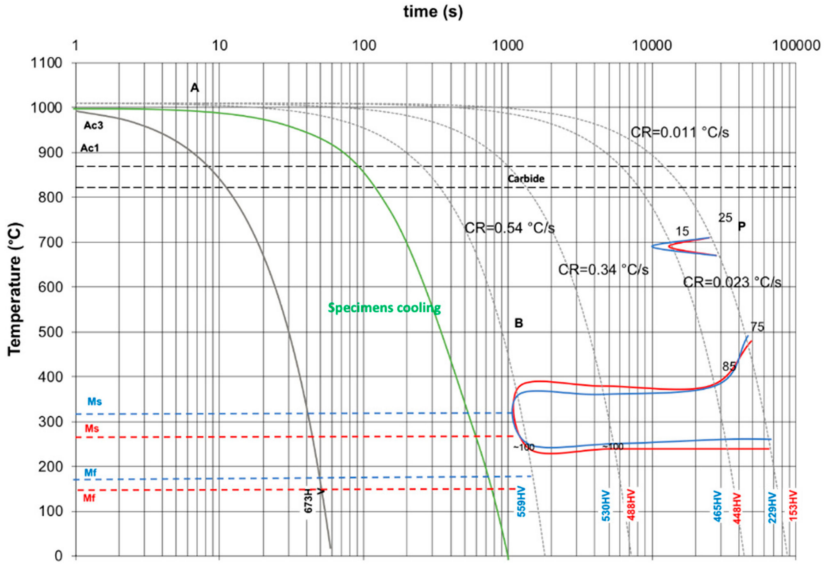

Figure 4. CCT diagrams of the considered steel (austenitization at 980 °C, blue curve; austenitization at 1200 °C, red curve). Green cooling curve: first cooling undergone by all specimens reported in Table 2.

The results show that, even if prior austenite grain size were quite different, significative differences are not found in the cooling behavior (Figure 5). In particular 10 and 75 µm grain sizes were measured in specimens after austenitization at 980 and 1200 °C, respectively. These results were expected following the high intrinsic steel hardenability due to the high C and Cr content.

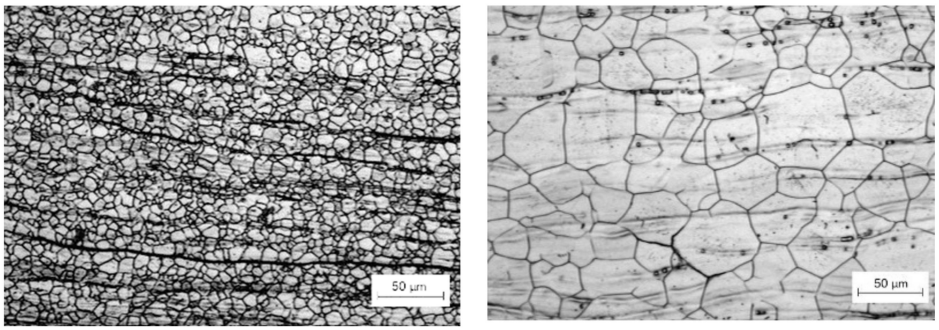

(**a**) (**b**)

Figure 5. Austenitic grain size of two specimens after austenitization at 980 °C (**a**) and 1200 °C (**b**).

3.2. Retained Austenite Evolution

Selected XRD spectra of specimens reported in Table 2 are shown in Figure 6. Even if retained austenite values are quite low, it is clear from the spectra reported in Figure 6 that it is possible to discriminate between specimens characterized by RA presence (e.g., Figure 6, specimen PT-γ-2) and specimens where XRD is not able to detect any RA (<2.0%) (e.g., Figure 6, specimen PT-γ-3). Retained austenite contents, as measured by means of XRD spectra analysis, are reported in Table 3. XRD measurements were confirmed, in selected cases, by phase maps analysis, as obtained by means of EBSD (Figure 7). In particular, 1.7% retained austenite content was measured in specimen PT-γ-2 by EBSD (to be compared to 2.5% as measured by XRD) and 1.2% in specimen PT-γ-3 (to be compared to <2.0% as measured by XRD). The low discrepancy obtained by EBSD with respect to XRD is justified by the two different adopted techniques [50]. The agreement between RA contents, as measured by the two different methods, makes the results reported in Table 3 consistent, even if their absolute values are quite low (in the proximity of XRD-technique sensitivity).

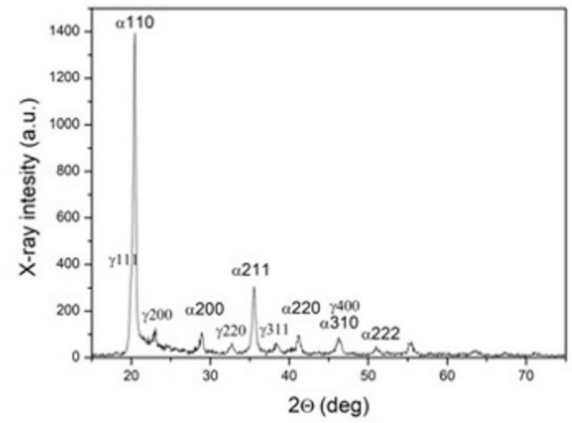

(**a**)

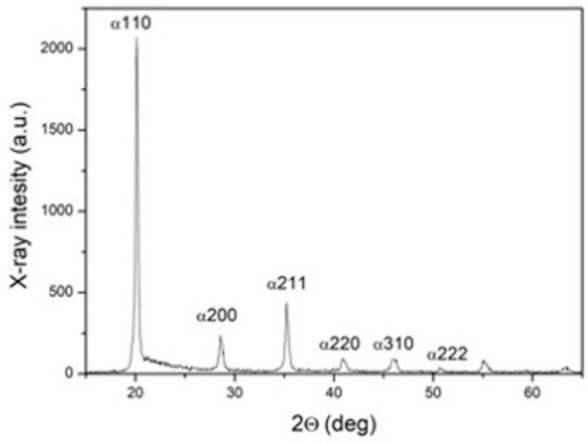

(**b**)

Figure 6. XRD spectra of selected heat-treated specimens: (**a**) specimen PT-γ-2 and (**b**) specimen PT-γ-3.

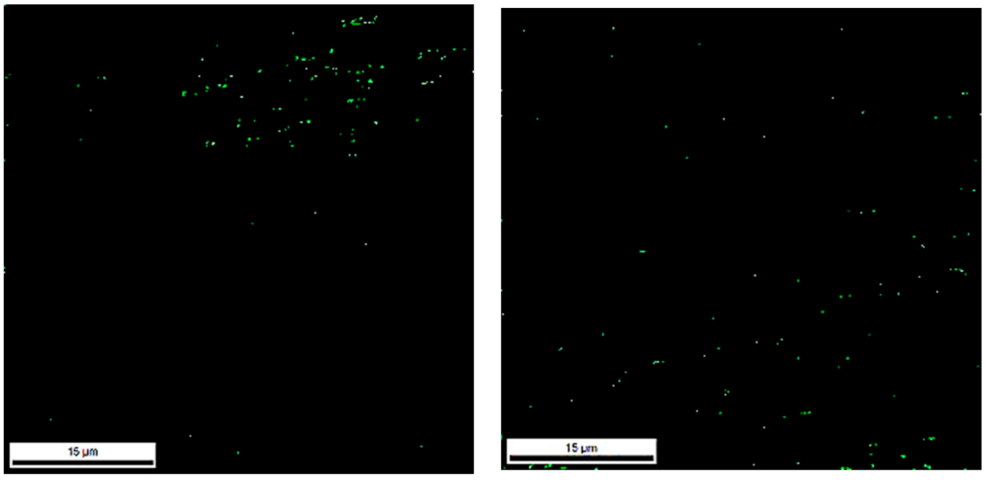

(**a**) (**b**)

Figure 7. Phase maps by EBSD (**a**) specimen PT-γ-2 and (**b**) specimen PT-γ-**3**. Green areas correspond to retained austenite.

Table 3. Retained austenite content as a function of performed heat treatments (three measures for each specimen are reported).

Specimen *n*.	RA (%)
Q & P	2.4; 2.4; 2.3
PT-γ-1	2.3; 2.2; 2.3
PT-γ-2	2.5; 2.6; 2.5
PT-γ-3	<2.0; 2.1; <2.0
PT-γ-4	2.1; 2.2; <2.0
PT-γ-5	2.6; 2.5; 2.5
PT-γ-6	2.2; 2.1; 2.3
PT-γ-7	<2.0; <2.0; 2.0
PT-γ-8	2.7; 3.0; 2.4
Q	2.1; 2.1; 2.0
Q & T	<2.0; 2.1; <2.0

Specimens *n*. PT-γ-3, PT-γ-7 and Q & T, double tempered at higher temperatures (>528 °C), show RA contents lower than 2.0%. All the other variants (reported in Table 3), with none or at a lower second tempering temperature, show higher RA contents. It is worth outlining that such results are independent from the microstructures obtained after cooling, according to Table 2. The other specimens show RA content ranging from 2.4% to 2.7%: such specimens were subjected to double tempering, but at a lower temperature (505 °C). The above considerations suggest that the double tempering heat treatment at higher temperatures (>528 °C) allows us to reactivate retained austenite that, during following cooling down to room temperature, decomposes in fine carbides

In fact, a very fine precipitation is detected in specimens PT-γ-3 and PT-γ-7 (average precipitation diameter d_p = 14.6 nm and d_p = 16.4 nm, respectively), as shown in Figure 8. Such precipitates were not detected in the other specimens. Finest precipitates (d_p < 10 nm) were identified to be chromium carbides vanadium rich. Vanadium presence was not detected in coarser precipitates. The crystallographic lattice parameters' measurements obtained by diffraction patterns analysis allowed us to identify precipitates ranging d_p < 5 nm as MC, precipitates ranging 5–10 nm as M_2C. The largest precipitates were classified as $M_{23}C_6$ (ranging 70–200 nm) and M_3C in the case of (d_p > 200 nm). The Brinell hardness HB dependence on retained austenite content is reported in Figure 9. Results show that higher hardness values are found in the case of higher-retained-austenite-content specimens (hence lower tempering temperature). Results suggest therefore that the presence of retained austenite, also in a small amount, should exert a non-negligible effect. This means that manufacturers are called for a specific heat-treatment design, depending on the final properties required for different forged components.

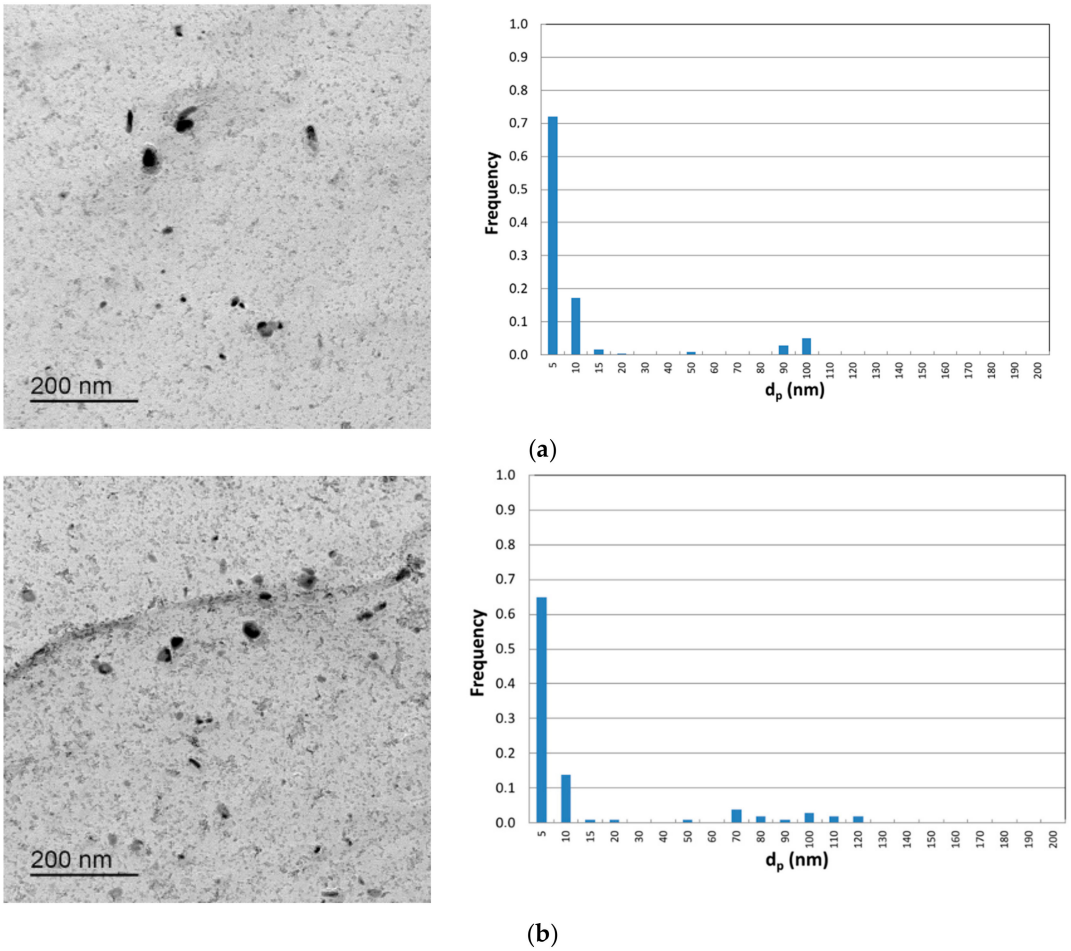

Figure 8. TEM images describing the precipitation state of (**a**) specimen PT-γ-3 and (**b**) specimen PT-γ-7.

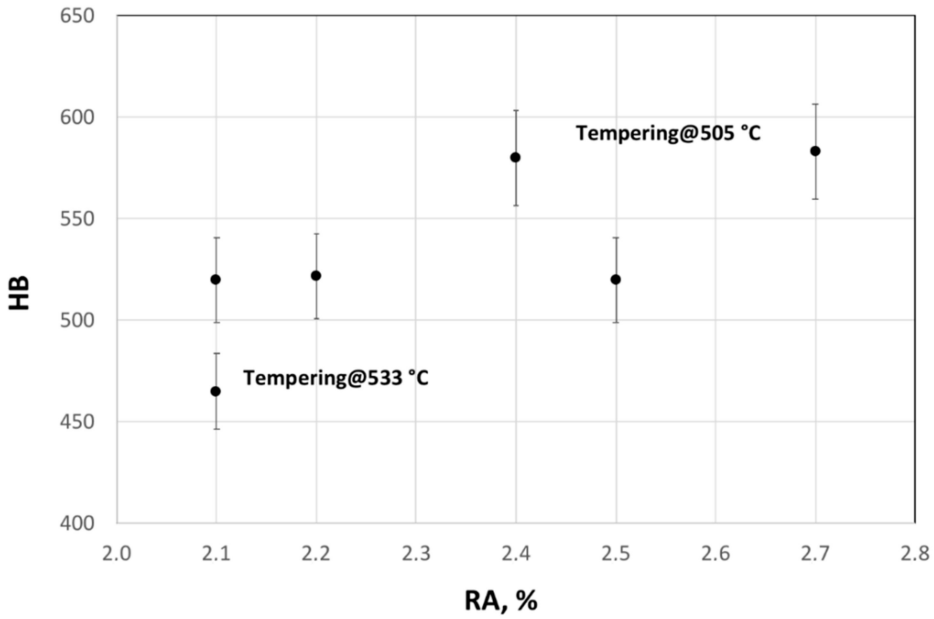

Figure 9. Hardness as a function of the retained austenite content.

4. Conclusions

In this paper, the heat treatment effect on a 7% Cr steel for forging was reported. Different heat treatments were considered, and microstructure evolution was analyzed. Heat treatments were designed with the aim of obtaining the following four microstructural families:

(1) Quenching and partitioning (specimen Q & P);
(2) Partially transformed austenite during a first quenching at 280 °C (specimens *n*. PT-γ-1 to PT-γ-4);
(3) Partially transformed austenite during a secondary cooling at 220 °C (specimens *n*. PT-γ-5 to PT-γ-8);
(4) 100% martensite (specimens Q just quenching, specimen Q & T quenching and tempering).

Results show the following:

(1) Retained austenite content is lower in double-tempered specimens at temperatures higher than 528 °C;
(2) The retained austenite disappeared after quenching down to room temperature and double tempering;
(3) The prior austenite grain size does not have an influence on the cooling behavior in this specific steel.

Author Contributions: Conceptualization, A.D.S.; methodology, A.D.S.; formal analysis, A.D.S. and C.T., formal analysis, A.D.S., C.T., and M.G. All authors have read and agreed to the published version of the manuscript.

Funding: This research received no external funding.

Conflicts of Interest: The authors declare no conflict of interest.

References

1. Changle, Z.; Hanguang, F.; Shengqiang, M.; Dawei, Y.; Jian, L.; Zhenguo, X.; Yongping, L. Effect of Mn content on microstructure and properties of wear-resistant bainitic steel. *Mater. Res. Express* **2019**, *6*, 1–22. [CrossRef]
2. Allain, S.; Bouaziz, O. Microstructure based modeling for the mechanical behavior of ferrite-pearlite steels suitable to capture isotropic and kinematic hardening. *Mater. Sci. Eng. A* **2008**, *496*, 329–336. [CrossRef]
3. De Andrés, C.G.; Capdevila, C.; Madariaga, I.; Gutierrez, I. Role of molybdenum in acicular ferrite formation under continuous cooling in a medium carbon microa-lloyed forging steel. *Scr. Mater.* **2001**, *45*, 709–716. [CrossRef]
4. Soffritti, C.; Merlin, M.; Vazsquez, R.; Fortini, A.; Garagnani, G.L. Failure analysis of worn valve train components of a four-cylinder diesel engine. *Eng. Fail. Anal.* **2018**, *92*, 528–538. [CrossRef]
5. Lee, K.S.; Yoon, D.H.; Kim, H.K.; Kwon, Y.-N.; Lee, Y.-S. Effect of annealing on the interface microstructure and mechanical properties of clad sheet. *Mater. Sci. Eng. A* **2012**, *556*, 319–330. [CrossRef]
6. Liu, C.Y.; Wang, Q.; Jia, Y.Z.; Jing, R.; Zhang, B.; Ma, M.Z.; Liu, R.P. Microstructures and mechanical properties of laminated composites prepared via warm roll bonding. *Mater. Sci. Eng. A* **2012**, *556*, 1–8. [CrossRef]
7. Di Schino, A.; Testani, C. Corrosion behavior and mechanical properties of AISI 316 stainless steel clad Q235 plate. *Metals* **2020**, *10*, 552. [CrossRef]
8. Morito, S.; Yoshida, H.; Maki, T.; Huang, X. Effect of block size on the strength of lath martensite in low carbon steels. *Mater. Sci. Eng. A* **2006**, *438*, 237–240. [CrossRef]
9. Fan, C.; Chen, M.M.; Chang, C.M.; Wu, W. Microstructure change caused by $(Cr,Fe)_{23}C_6$ carbides in high chromium Fe-Cr-C alloys. *Surf. Coat. Technol.* **2006**, *201*, 908–912. [CrossRef]
10. Akbarzadeh, A.; Naghdy, S. Hot workability of high carbon high chromium tool steel. *Mater. Des.* **2013**, *46*, 654–659. [CrossRef]
11. Di Schino, A.; Di Nunzio, P.E.; Turconi, G.L. Microstructure evolution during tempering of martensite in medium carbon steel. In *Materials Science Forum*; Trans Tech Publications Ltd.: Stafa-Zurich, Switzerland, 2007; Volume 558, pp. 1435–1441.
12. Di Schino, A. Manufacturing and application of stainless steels. *Metals* **2020**, *10*, 327. [CrossRef]

13. Di Schino, A. Analysis of heat treatment effect on microstructural features evolution in a micro-alloyed martensitic steel. *Acta Metall. Slovaca* **2016**, *22*, 266–270. [CrossRef]
14. Di Schino, A.; Kenny, J.M.; Abbruzzese, G. Analysis pf the recrystallization and grain growth processes in AISI 316 stainless steel. *J. Mater. Sci.* **2002**, *37*, 5291–5298. [CrossRef]
15. Di Schino, A.; Alleva, L.; Guagnelli, M. Microstructure evolution during quenching and tempering of martensite in a medium C steel. In *Materials Science Forum*; Trans Tech Publications Ltd.: Stafa-Zurich, Switzerland, 2007; Volume 715, pp. 860–865.
16. Mohammed, M.N.; Omar, M.Z.; Zubaidi, S. Microstructure and mechanical properties of tool steels. *Metals* **2018**, *8*, 316. [CrossRef]
17. Di Schino, A.; Di Nunzio, P.E. Metallurgical aspects related to contact fatigue phenomena in steels for back up rolling. *Acta Metall. Slovaca* **2017**, *23*, 62–71. [CrossRef]
18. Pezzato, L.; Gennari, C.; Chukin, D.; Toldo, M.; Sella, F.; Toniolo, M.; Zambon, A.; Brunelli, K.; Dabalà, M. Study of the effect of multiple tempering on the impact toughness of forged S690 structural steel. *Metals* **2020**, *10*, 507. [CrossRef]
19. Bhadeshia, H.K.D.H.; Honeycombe, R.W.K. *Steels: Microstructure and Properties*; Butterworths Heinemann (Elsevier): Aalborg, Denmark, 2006; ISBN 9780750680844.
20. Di Schino, A.; Valentini, L.; Kenny, J.M.; Gerbig, Y.; Ahmed, I.; Hefke, H. Wear resistance of high-nitrogen austenitic stainless steel coated with nitrogenated amorphous carbon films. *Surf. Coat. Technol.* **2002**, *161*, 224–231. [CrossRef]
21. Napoli, G.; Di Schino, A.; Paura, M.; Vela, T. Colouring titanium alloys by anodic oxidation. *Metalurgija* **2018**, *57*, 111–113.
22. Li, Z.; Jia, P.; Liu, Y.; Qi, H. Carbide Precipitation, Dissolution, and Coarsening in G18CrMo2–6 Steel. *Metals* **2019**, *9*, 916. [CrossRef]
23. Sharma, D.K.; Filipponi, M.; Di Schino, A.; Rossi, F.; Castaldi, J. Corrosion behaviour of high temeperature fuel cells: Issues for materials selection. *Metalurgija* **2019**, *58*, 347–351.
24. Qin, S.; Song, R.; Xiong, W.; Liu, Z.; Wang, Z.; Guo, K. Microstructure evolution and mechanical properties of grade E690 offshore platform steel. In *HSLA Steels 2015, Microalloying 2015 & Offshore Engineering Steels 2015*; John Wiley & Sons, Inc.: Hoboken, NJ, USA, 2015; Volume 2, pp. 1117–1123. ISBN 9781119223399.
25. Maropoulos, S.; Ridley, N.; Karagiannis, S. Structural variations in heat treated low alloy steel forgings. *Mater. Sci. Eng. A* **2004**, *380*, 79–92. [CrossRef]
26. Bregliozzi, G.; Ahmed, S.I.-U.; Di Schino, A.; Kenny, J.M.; Haefke, H. Friction and Wear Behavior of Austenitic Stainless Steel: Influence of Atmospheric Humidity, Load Range, and Grain Size. *Tribol. Lett.* **2004**, *17*, 697–704. [CrossRef]
27. Rufini, R.; Di Pietro, O.; Di Schino, A. Predictive simulation of plastic processing of welded stainless steel pipes. *Metals* **2018**, *8*, 519. [CrossRef]
28. Kobayashi, Y.; Tanaka, Y.; Matsuoka, K.; Kinoshita, K.; Miyamoto, Y.; Murata, H. Effect of forging ratio and grain size on tensile and fatigue strength of pure titanium forgings. *J. Soc. Mater. Sci.* **2005**, *54*, 66–72. [CrossRef]
29. Zhu, K.; Qu, S.; Feng, A.; Sun, J.; Shen, J. Microstructural evolution and refinement mechanism of alloy during multidirectional isothermal forging. *Materials* **2019**, *12*, 2496. [CrossRef] [PubMed]
30. Padap, A.K.; Chaudhari, G.P.; Nath, S.K.; Pancholi, V. Ultrafine-grained steel fabricated using warm multiaxial forging: Microstructure and mechanical properties. *Mater. Sci. Eng. A* **2009**, *527*, 110–117. [CrossRef]
31. Wang, B.; Liu, Z.; Li, J.; Chaudhari, G.P. Microstructure evolution in AISI201 austenitic stainless steel during the first compression cycle of multi-axial compression. *Mater. Sci. Eng. A* **2013**, *568*, 20–24. [CrossRef]
32. Soleymani, V.; Eghbali, B.; Chaudhari, G.P. Grain refinement in a low carbon steel through multidirectional forging. *J. Iron Steel Res. Int.* **2012**, *19*, 74–78. [CrossRef]
33. Padap, A.K.; Chaudhari, G.P.; Pancholi, V.; Nath, S.K. Warm multiaxial forging of AISI 1016 steel. *Mater. Des.* **2010**, *31*, 3816–3824. [CrossRef]
34. Ghosh, S.; Singh, A.K.; Mula, S. Effect of critical temperatures on microstructures and mechanical properties of Nb-Ti stabilized IF steel processed by multiaxial forging. *Mater. Des.* **2016**, *100*, 47–57. [CrossRef]
35. Zrnik, J.; Kvackaj, J.; Pongpaybul, A.; Sricharoenchai, P.; Vilk, J.; Vrchivinsky, V. Effect of thermomechanical processing on the microstructure and mechanical properties of Nb-Ti microalloyed steel. *Mater. Sci. Eng. A* **2001**, *319*, 321–325. [CrossRef]

36. De Ardo, A.I.; Garcia, C.I.; Hua, M. Micro-alloyed steels for high strength forgings. *Metall. Ital.* **2010**, *102*, 5–10.
37. Opiela, M. Effect of Thermomechanical Processing on the Microstructure and Mechanical Properties of Nb-Ti-V micro-alloyed Steel. *J. Mat. Eng. Perf.* **2014**, *23*, 3379–3388. [CrossRef]
38. Di Schino, A. Analysis of phase transformation in high strength low alloyed steels. *Metalurgija* **2017**, *56*, 349–352.
39. Zitelli, C.; Mengaroni, S.; Di Schino, A. Vanadium micro-alloyed high strength steels for forgings. *Metalurgija* **2017**, *56*, 326–328.
40. Mancini, S.; Langellotto, L.; Di Nunzio, P.E.; Zitelli, C.; Di Schino, A. Defect reduction and quality optimisation by modelling plastic deformation and metallurgical evolution in ferritic stainless steels. *Metals* **2020**, *10*, 186. [CrossRef]
41. Bendick, W.; Ring, M. Creep rupture strength of tungsten-alloyed 9–12% Cr steels for piping in power plant. *Steel Res.* **1996**, *67*, 382–397. [CrossRef]
42. Haarman, K.; Bendicl, W.; Arbaba, A. *The T91/P91 Book*, 2nd ed.; Vallourec and Mannesmann Tubes: Boulogne-Billancourt, France, 2002.
43. Garr, K.; Rhodes, C.; Kramer, D. Effects of microstructure on swelling and tensile properties of neutron irradiated Types 316 and 405 stainless steels. *ASTM Spec. Tech. Publ.* **1973**. [CrossRef]
44. Zitelli, C.; Folgarait, P.; Di Schino, A. Laser powder bed fusion of stainless-steel grades: A review. *Metals* **2019**, *9*, 731. [CrossRef]
45. Abe, F.; Horiuchi, T.; Taneike, M.; Sawada, K. Stabilization of martensitic microstructure in advanced 9Cr steel during creep at high temperature. *Mater. Sci. Eng. A* **2004**, *378*, 299–303. [CrossRef]
46. Caballero, F.; Alvarez, L.; Capdevila, C.; de Andrés, C.G. The origin of splitting phenomena in the martensitic transformation of stainless steels. *Scr. Mater.* **2003**, *49*, 315–320. [CrossRef]
47. Barlow, L.; Du Toit, M. Effect of austenitizing heat treatment on the microstructure and hardness of martensitic stainless steel AISI 420. *J. Mater. Eng. Perform.* **2012**, *1*, 1327–1336. [CrossRef]
48. Tao, X.G.; Gu, J.F.; Han, L.Z. Carbonitride dissolution and austenite grain growth in a high Cr ferritic heat-resistant steel. *ISIJ Int.* **2014**, *54*, 1704–1715. [CrossRef]
49. Chintan, S. Quenching and Partitioning Process of Grade P91 Steel. Master's Thesis, Texas University, Austin, TX, USA, 2018.
50. Pashangeh, S.; Zarchi, H.R.K.; Banadkouki, S.S.G.; Somani, M. Detection and Estimation of Retained Austenite in a High Strength Si-Bearing Bainite-Martensite-Retained Austenite Micro-Composite Steel after Quenching and Bainitic Holding (Q & B). *Metals* **2019**, *9*, 492.